Biophysical Journal Volume 86 April 2004 2329–2341

Bifunctional Rhodamine Probes of Myosin Regulatory Light Chain Orientation in Relaxed Skeletal Muscle Fibers

Andrew S. Brack,* Birgit D. Brandmeier,† Roisean E. Ferguson,† Susan Criddle,* Robert E. Dale,* and Malcolm Irving*

*School of Biomedical Sciences, Guy's Campus, King's College London, London SE1 1UL, United Kingdom; and
†National Institute for Medical Research, London NW7 1AA, United Kingdom

ABSTRACT The orientation of the regulatory light chain (RLC) region of the myosin heads in relaxed skinned fibers from rabbit psoas muscle was investigated by polarized fluorescence from bifunctional rhodamine (BR) probes cross-linking pairs of cysteine residues introduced into the RLC. Pure 1:1 BR-RLC complexes were exchanged into single muscle fibers in EDTA rigor solution for 30 min at 30°C; ~60% of the native RLC was removed and stoichiometrically replaced by BR-RLC, and >85% of the BR-RLC was located in the sarcomeric A-bands. The second- and fourth-rank order parameters of the orientation distributions of BR dipoles linking RLC cysteine pairs 100-108, 100-113, 108-113, and 104-115 were calculated from polarized fluorescence intensities, and used to determine the smoothest RLC orientation distribution—the maximum entropy distribution—consistent with the polarized fluorescence data. Maximum entropy distributions in relaxed muscle were relatively broad. At the peak of the distribution, the "lever" axis, linking Cys^{707} and Lys^{843} of the myosin heavy chain, was at 70–80° to the fiber axis, and the "hook" helix (Pro^{830}–Lys^{843}) was almost coplanar with the fiber and lever axes. The temperature and ionic strength of the relaxing solution had small but reproducible effects on the orientation of the RLC region.

INTRODUCTION

Extrinsic dipole probes have been widely used to investigate functionally significant changes in the conformation of protein domains. This approach can complement high resolution in vitro methods like x-ray crystallography and NMR by providing structural information from protein domains in their native environment. Such information allows changes in domain orientations to be studied in large macromolecular complexes under physiological conditions. Moreover, the high time resolution of the method allows dynamic studies of structural changes in response to cellular signals. The power of these dipole probe techniques is greatly enhanced if the relative orientation of the dipole with respect to the domain backbone is known, and two methods to achieve this have recently been described. One of these depends on a small fluorophore bound to the n, $n + 1$, $n + 4$, and $n + 5$ cysteine mutant of an α-helical region of the domain (Griffin et al., 1998). The other, used in this work, depends on cross-linking pairs of cysteines with a bifunctional rhodamine (BR) (Corrie et al., 1999).

The bifunctional rhodamine approach was initially applied to the myosin regulatory light chain (RLC) in skeletal muscle fibers (Corrie et al., 1999; Hopkins et al., 2002). RLC mutants were expressed containing pairs of solvent-accessible cysteines 10–15 Å apart (Fig. 1). The two cysteines were reacted with a bis-iodoacetamidorhodamine (BR-I_2; Corrie et al., 1998), and pure 1:1 cross-linked BR-RLC complexes were isolated (Corrie et al., 1999). These BR-RLCs were exchanged for the native RLCs in demembranated single fibers from rabbit psoas muscle. Polarized fluorescence intensity measurements on these labeled fibers were used to characterize the orientation of the BR dipole, and thus that of the line joining the cysteines to which it was attached, with respect to the muscle fiber axis. Orientation data from four different cysteine pairs in the same region of the RLC, residues 100-108, 104-115, 100-113, and 108-113 (Fig. 1), were combined to describe the three-dimensional orientation of the RLC region.

The focus of previous BR-RLC studies (Corrie et al., 1999; Hopkins et al., 2002) was to describe the changes in the orientation of the RLC region associated with sliding between the actin and myosin filaments and with active force generation in muscle. These changes are fundamental to understanding the mechanism of the myosin motor, because the RLC is located in the so-called ''lever arm'' region of the myosin head (Fig. 1) that is thought to tilt during the generation of force or filament sliding (Rayment et al., 1993a,b; Irving et al., 1995; Dominguez et al., 1998; Geeves and Holmes, 1999). The BR-RLC studies showed that the lever arm did tilt but that the average orientation change was small, suggesting that only a small fraction of the myosin heads in the fiber participated in active force generation in the conditions of those experiments.

The broader significance of those results depends on the extent to which the BR-RLC probes report RLC orientation accurately, without modifying its structure or function. In vitro characterization of the BR-RLCs by tryptic digestion and mass spectrometry (Corrie et al., 1999) established that the required conjugates had been synthesized and purified

Submitted September 17, 2003, and accepted for publication December 1, 2003.

Address reprint requests to Professor Malcolm Irving, Randall Centre, School of Biomedical Sciences, Guy's Campus, King's College London, London SE1 1UL, UK. E-mail: malcolm.irving@kcl.ac.uk.

0006-3495/04/04/2329/13 $2.00

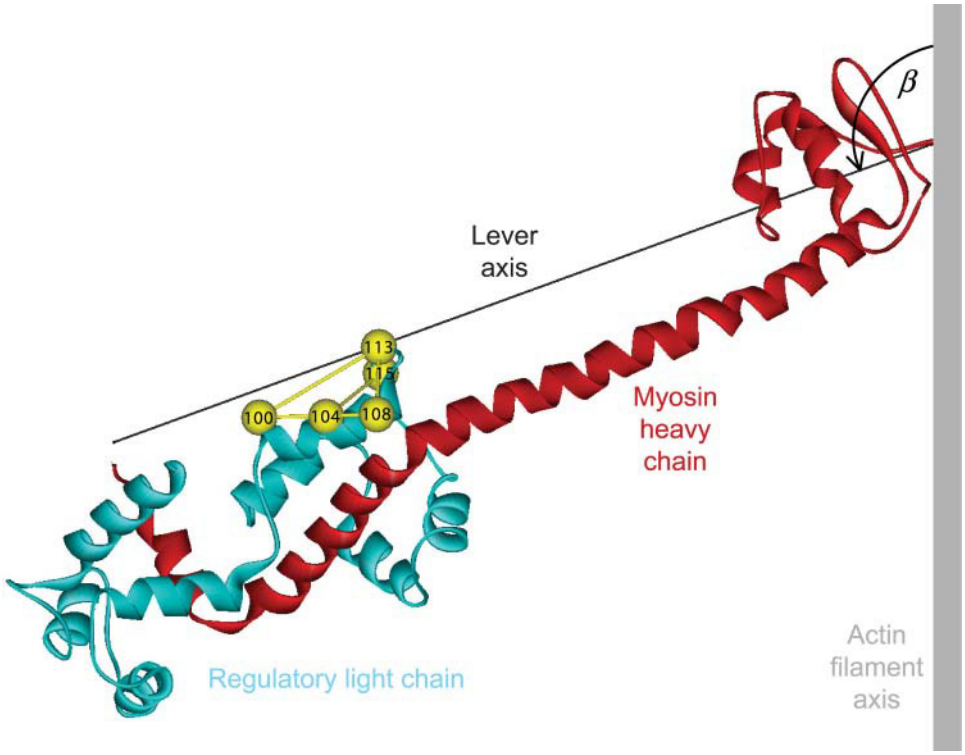

FIGURE 1 Ribbon representation of the lever arm region of the myosin head. The myosin heavy chain from Cys^{707} on the right to Lys^{843} on the left is shown in red. The lever arm axis joins the α-carbons of these residues, and the hook helix is the short helix on the left. Pairs of cysteine residues in the regulatory light chain (*blue*) that were cross-linked by bifunctional rhodamine are shown as yellow spheres joined by rods. The orientation of the lever arm region shown corresponds to $\beta = 110°$, $\gamma = 20°$, the peak of the orientation distribution in Fig. 6 *A*. Prepared with ViewerPro (Accelrys, San Diego, CA) with coordinates from Rayment et al. (1993b). The essential light chain has been omitted for clarity.

successfully. Competitive binding assays and Mg^{2+}-ATPase assays in myofibrils provided strong evidence that the BR-RLCs fold normally, and bind to the myosin heavy chain in a functional conformation (Corrie et al., 1999). The NMR structure of a closely related protein domain, the N-terminal lobe of troponin C, with BR cross-linking two cysteine residues, showed directly that the domain structure was not altered by BR labeling (Mercier et al., 2003).

Here we investigated the incorporation of the BR-RLCs into demembranated muscle fibers. The fraction of the native RLC in the fiber that is replaced by BR-RLC and the location of BR-RLC in the sarcomere were determined by fluorescence intensity measurements, confocal microscopy, and gel electrophoresis. We also used polarized intensity measurements from the BR-RLCs to investigate the orientation of the RLC region in relaxed muscle fibers, focusing on two interventions that are expected to produce substantial changes in the conformations of the myosin heads. The temperature was raised from 5°C to 20°C to induce helical ordering of the myosin heads on the surface of the myosin filaments (Wray, 1987; Lowy et al., 1991; Xu et al., 1997, 1999), and the ionic strength of the relaxing solution was lowered to promote weak binding of myosin heads to actin. This weakly bound state is of interest because of its potential similarity to an early intermediate in the force-generating interaction between myosin, actin, and ATP (Eisenberg and Hill, 1985; Kraft et al., 1995; Xu et al., 1997).

METHODS

Expression of myosin regulatory light chain mutants

Mutants of chicken gizzard regulatory light chain (cgRLC) with cysteines at positions 100-108, 104-115, 100-113, and 108-113 were obtained by site-directed mutagenesis, using the general methods described by Taylor et al. (1985). All mutations were checked by DNA sequencing and later by mass spectrometry of the expressed proteins. Wild-type cgRLC has a single cysteine (Cys^{108}) and the 100-108 and 108-113 double-cysteine mutants were produced by the mutations D100C and A113C, respectively. The 100-113 double-cysteine RLC was made by combining these with C108A, whereas the 104-115 double-cysteine RLC was made by the mutations C108A, N104C, and G115C. Each mutant protein was expressed in the pSJW1 vector (Winder and Kendrick-Jones, 1995). The expression vector was transformed into Ca^{2+}-competent *Escherichia coli* BL21 (DE3) cells, that were then spread onto Luria Broth agar plates containing 100 μg/ml ampicillin and grown overnight at 37°C. Typically, 2 L of Luria Broth medium containing 100 μg/ml ampicillin was inoculated from these plates, and cells were grown overnight at 34°C. The cells were harvested by centrifugation and resuspended in 80 ml of lysis buffer (25% w/v sucrose, 2 mM EDTA, 2 mM EGTA, 3 mM sodium azide, 0.5 mM phenylmethylsulfonyl fluoride (PMSF), 5 mM dithiothreitol (DTT), 50 mM Tris-HCL, pH 8.0), frozen in liquid nitrogen and stored at –20°C. For subsequent isolation of inclusion bodies that contained the expressed RLC, the thawed mixture was homogenized, supplemented with 100 mg lysozyme, 1 mg DNase, 10 mM $MgCl_2$, and 1 mM $MnCl_2$, and incubated at room temperature for 30 min. The incubate was diluted with 2 vol of 200 mM NaCl, 1% deoxycholate, 1.6% Nonidet P40, 2 mM EDTA, 20 mM Tris-HCl, pH 7.5, and the mixture was stirred at 4°C for 30 min, then centrifuged (26000 $\times$ *g* for 20 min). The pelleted inclusion bodies were suspended in 100 ml of 0.5% Triton X-100, 1 mM EDTA, 10 mM Tris-HCl, pH 8.0 (wash

buffer) that was supplemented with 0.5 mg DNase, 10 mM $MgCl_2$, 1 mM $MnCl_2$. The mixture was incubated at room temperature for 25 min, centrifuged (26000 × *g* for 12 min at 4°C), and the pellet was resuspended in 100 ml wash buffer, then incubated and centrifuged as above. The pellet was homogenized in wash buffer, diluted to 200 ml in the same buffer, and centrifuged (26000 × *g*, 4°C, 7 min). The final pellet was dispersed in 10–20 ml buffer containing 25% sucrose, 2 mM EDTA, 2 mM EGTA, 3 mM sodium azide, 1 mM PMSF, 10 mM DTT, 50 mM Tris-HCL, pH 8.0 with one Complete protease inhibitor cocktail tablet (Roche Diagnostics, Lewes, UK) per 50 ml, frozen in liquid nitrogen and stored at –20°C.

To isolate RLCs, one half of the inclusion body preparation was solubilized by addition of sufficient urea to attain a 6 M concentration in twice the volume of the initial suspension. After dissolution of the urea, the volume was adjusted to twice its initial value by adding a solution calculated to give final concentrations of 2 mM DTT (ignoring the DTT initially present), 2 mM $MgCl_2$, and 25 mM Tris-HCL, pH 7.5. The material was clarified by centrifugation and the RLC was purified from the supernatant on a 100-mL DE52 anion exchange column (Whatman, Maidstone, UK) at 4°C, using a 50-175 mM NaCl gradient in 6 M urea, 1 mM $MgCl_2$, 1 mM DTT, 25 mM Tris-HCL, pH 7.5 in a total volume of 1 L. Each RLC eluted at 90–100 mM NaCl and fractions were analyzed for purity using 15% SDS-PAGE. Pure fractions were pooled and concentrated by ultrafiltration through an Amicon (Millipore, Billerica, MA) PM10 membrane to 10–20 mg/ml, dialyzed at 4°C against storage buffer (100 mM NaCl, 2 mM Mg^{2+}, 1 mM DTT, 25 mM Tris-HCl, pH 8.0) (2 × 5 L each for 2 h, then 5 L overnight). The dialysis bag was then placed on a bed of solid sucrose and the cgRLC concentrated to ~25 mg/ml before storage at –20°C. Protein concentration was determined using a calculated extinction coefficient of 3840 M^{-1} cm^{-1} at 280 nm (Gill and von Hippel, 1989).

Preparation of BR-RLCs

An aliquot of the stock solution of mutant cgRLC (~50 mg protein) was incubated with 5 mM DTT at room temperature for 30 min to reduce disulfides formed during storage and gel filtered (PD-10 column, Amersham Biosciences, Uppsala, Sweden) into labeling buffer (25 mM Tris-HCl, 100 mM NaCl, 1 mM $MgCl_2$, pH 7.4). The eluted RLC was diluted to 1 mg/ml (50 μM) in labeling buffer. Tris(carboxyethyl)phosphine (50 μM final concentration) was added to maintain the protein in its reduced form, followed by 30 μM BR-I_2 (added from a stock 15–20 mM solution in dimethylformamide). The solution was incubated at room temperature, and further 20-μM aliquots of BR-I_2 were added every 10 min to a final concentration of 90 μM. A small aliquot (~6 μg protein) was removed 20 min after the final addition, and quenched with 3 mM (final concentration) of sodium 2-mercaptoethanesulfonate. The extent of reaction was determined by analytical reverse-phase high-performance liquid chromatography (HPLC) (C18 Vydac column, Hichrom, Theale, UK) with a linear gradient from 60% solvent A (H_2O/0.1% trifluoroacetic acid) and 40% solvent B (acetonitrile/0.082% trifluoroacetic acid) to 40% solvent A and 60% solvent B over 20 min at a flow rate of 1 ml/min. Elution was monitored by absorbance at 215 nm and rhodamine fluorescence (λ_{ex} 549 nm, $\lambda_{em} > 580$ nm). Generally the desired BR-RLC, in which both cysteines were cross-linked by one BR, could be resolved from unlabeled RLC and from RLC in which the cysteines had reacted with 2 BRs. When an optimal level of the 1:1 protein/BR conjugate was obtained, the reaction was quenched by the addition of 3 mM sodium 2-mercaptoethanesulfonate (final concentration). The resulting solution was gel filtered through PD-10 columns (total sample vol 2.5 ml/column) into fast-protein liquid chromatography (FPLC) buffer (10 mM potassium phosphate, 50 mM potassium propionate (KPr), 1 mM $MgCl_2$ at pH 7.0) to remove unconjugated dye.

BR-RLCs were purified in 6−8-mg batches on a Mono-S HR 10/10 FPLC cation exchange column (Amersham Biosciences) using a 150–300 mM KCl gradient (total volume 150 ml) at 2.5 ml min^{-1}. Fractions eluting at ~200 mM KCl were analyzed by reverse-phase HPLC (as described above) and combined to give a pooled fraction, typically of ~90% purity. The typical yield of purified, labeled protein was 10%. Fractions containing pure labeled protein were concentrated against solid sucrose, as described above, to a final concentration of 1–1.5 mg/ml. The protein concentration was measured using an extinction coefficient for the rhodamine of 52,000 M^{-1} cm^{-1} at 528 nm (Corrie et al., 1998), based on 1:1 stoichiometric labeling that was confirmed for each labeled RLC by electrospray mass spectrometry and limited tryptic digestion (Corrie et al., 1999). Two-site attachment of BR gives two diastereoisomeric-labeled proteins because of restricted rotation of the carboxy-substituted phenyl ring with respect to the xanthene ring system that comprises the fluorophore. HPLC analysis of 108-BR-113 and 104-BR-115 revealed two labeled peaks, each of the same measured mass and therefore attributed to the presence of diastereoisomers that were chromatographically distinct in these cases. In the case of 108-BR-113, these diastereoisomers were separable by FPLC and were each found to give similar polarized fluorescence results (Corrie et al., 1999).

Muscle fiber preparation and incorporation of BR-RLC

Single fibers were prepared from psoas muscles of New Zealand white rabbits as described previously (Sabido-David et al., 1998a). Fiber bundles were stored at –20°C in a solution containing 70 mM KPr, 8 mM Mg acetate (MgAc), 5 mM K_2EGTA, 7 mM Na_2ATP, 6 mM imidazole, 1 mM NaN_3, 0.1 mM PMSF, 0.1 mg/ml soybean trypsin inhibitor, 8 μg/ml leupeptin, and 50% glycerol, pH 7.0. Fibers were used within 4 weeks.

Single-fiber segments, 2–3 mm long, were dissected from a bundle and aluminum T-clips were crimped to each end of the segment. The fiber was mounted horizontally in a 70-μl glass trough containing relaxing solution (in mM: imidazole, 25; K_2EGTA, 5.0; MgAc, 7; KPr, 80; Na_2ATP, 5; sodium creatine phosphate (NaCP), 5; pH 7.0; 159 mM ionic strength) on a temperature-controlled microscope stage, and attached to a force transducer as described previously (Sabido-David et al., 1998a). Sarcomere length and fiber diameter were measured with a 32× objective. Fiber length was adjusted to set the sarcomere length to 2.4 μm except where noted.

Each BR-RLC was separately incorporated into single fibers at 50 μM in exchange solution (20 mM K_2EDTA, 10 mM potassium phosphate (KP_i), 50 mM KPr, pH 7.0, 150 mM ionic strength) for 30 min at 30°C (Sabido-David et al., 1998a), except where noted. Troponin and troponin C lost in the exchange process were replaced in relaxing solution. The preactivating solution, in which fibers were incubated for 2 min before activation, contained (in mM): imidazole, 25; K_2EGTA, 0.2; MgAc, 7; KPr, 90; Na_2ATP, 5; NaCP, 5; pH 7.0; creatine phosphokinase (Sigma, St. Louis, MO), 1 mg/ml; 155 mM ionic strength. Activating solution (pCa 4.5) contained (in mM): imidazole, 25; MgAc, 7; KPr, 40; Na_2ATP, 5; NaCP, 10; CaEGTA, 10; pH 7.0; creatine phosphokinase, 1 mg/ml; 150 mM ionic strength. Low ionic strength relaxing solution contained (in mM): imidazole, 7; K_2EGTA, 2; MgAc, 2.1; KPr, 0.7; Na_2ATP, 1.1; pH 7.0, 20 mM ionic strength. Rigor solution contained (in mM): imidazole, 10; K_2EGTA, 2.5; MgAc, 2.2; KPr, 130.0; pH 7.0, 151 mM ionic strength.

Fluorescence polarization

Fluorescence emission from the BR-RLC in a muscle fiber was collected by a 0.25 numerical aperture objective in a modified epifluorescence microscope, and separated into components polarized parallel and perpendicular to the muscle fiber axis (Sabido-David et al., 1998a). The intensities of these components, $I_{\parallel}$ and $I_{\perp}$, respectively, were measured with two photomultipliers. Fluorescence was alternately excited along two illumination pathways. Excitation light (540 nm; 30 nm FWHM) propagating in line with the emitted light (''*x* illumination'') was directed onto the fiber through the objective of the epifluorescence microscope by a dichroic mirror (Sabido-David et al., 1998a). Excitation light propagating at 90° to both the direction of the emitted light and the fiber axis (''*y* illumination''; Hopkins et al., 1998; Dale et al., 1999) was provided by

a 532-nm helium-neon laser focused at the fiber by an $f = 40$ mm lens. Both the x and y illumination could also be polarized either parallel or perpendicular to the fiber axis, so in total eight polarized intensities were measured: ${}^{x}_{\|}I_{\|}$, ${}^{x}_{\|}I_{\perp}$, ${}^{x}_{\perp}I_{\|}$, ${}^{x}_{\perp}I_{\perp}$, ${}^{y}_{\|}I_{\|}$, ${}^{y}_{\|}I_{\perp}$, ${}^{y}_{\perp}I_{\|}$, and ${}^{y}_{\perp}I_{\perp}$, where the presubscript denotes the polarization of the x or y illumination (presuperscript). For fluorophores like rhodamine with collinear absorption and emission dipoles. these eight intensities can be reduced to three independent order parameters that contain all the information about the dipole orientation that is available from steady-state polarized intensity measurements: $\langle P_{2d} \rangle$, $\langle P_2 \rangle$, and $\langle P_4 \rangle$ (Dale et al., 1999).

RLC orientation distributions were calculated by combining the order parameters from a set of BR-RLCs using maximum entropy analysis (van der Heide et al., 2000). The orientations of the BR-RLC dipoles in the coordinate frame of the RLC region were calculated from the atomic coordinates of the β-carbons of the residues replaced by cysteines in the crystallographic structure of the head region of chicken skeletal myosin (Rayment et al., 1993b) as described by Hopkins et al. (2002). A ''lever'' axis was defined as a line joining the α-carbons of Cys^{707} and Lys^{843} of the myosin heavy chain (Fig. 1), and a ''hook'' axis as the line joining the midpoints between the pairs Phe^{836}-Ile^{838} and Met^{832}-Leu^{834}. The angular coordinates of the 100-BR-108, 108-BR-113, 104-BR-115, and 100-BR-113 dipoles in this frame are: $\theta = 21.9°$, 72.04°, 56.04°, and 21.86°; $\phi = -167.16°$, 21.40°, 59.54°, and 28.01°, respectively, where θ is the angle between the dipole and lever axes and ϕ is the angle between the lever-dipole plane and the lever-hook plane. An increase in ϕ denotes a counterclockwise rotation of the dipole around the lever axis as viewed from Lys^{843}. The orientation of the RLC region with respect to the muscle fiber axis is defined by the angle β between the lever axis and fiber axis (Fig. 1), and the angle γ that describes rotation of the RLC region around the lever axis. An increase in β is defined as producing translation of Lys^{843} toward the Z-line of the half-sarcomere (the direction of muscle shortening). When $\gamma = 0$, the hook axis is coplanar with the lever and fiber axes, and its Lys^{843} end points toward the sarcomeric M-line; increasing γ denotes counterclockwise rotation of the RLC region as viewed from Lys^{843}.

Confocal microscopy

Fibers were stretched to a sarcomere length of ~4.0 μm in relaxing solution, and the T-clips at each end of the fiber were glued to a microscope slide. Fibers were fixed in 4% (w/v) paraformaldehyde in phosphate-buffered saline, and transferred to 5% (w/w) diazabicyclooctane in glycerol for 15 min to minimize fluorescence fading. Confocal images were obtained using a Leica DM RBE microscope (Leica, Heidelberg, Germany) with a krypton laser source (568 nm), 580 nm beam splitter, 590 nm long pass filter, and 63× (numerical aperture 1.3) oil-immersion objective. A series of optical sections at 10-μm intervals through the fiber depth was collected; the order of image collection at the different depths was randomized and three images were collected at each depth from each fiber. The images were analyzed either using software provided with the microscope (Leica TCS NT version 1.6.587), or using the program hv (A. Stewart, Brandeis University), with similar results. The linearity of the recorded fluorescence intensities was checked using a series of rhodamine standards.

SDS-PAGE

Procedures for SDS-PAGE of extracts from single muscle fibers were based on those described by Moss et al. (1983). Two 2-mm segments were dissected from adjacent regions of each single fiber; one was kept as a control and the other used for BR-RLC exchange as described above. Each segment was then transferred to 20-μl sample buffer (21% glycerol, 1.5% sodium dodecyl sulfate, 44 mM Tris-HCl, 0.03% bromophenol blue, 0.032% DTT, pH 6.8) and sonicated for 5 min at 80°C. Samples were analyzed by 13.5% acrylamide SDS-PAGE (250 V, 25 mA, 7 h). The gels were silver-stained as described by Giulian et al. (1983) and scanned with a GS-690 densitometer (Bio-Rad, Hercules, CA). Gel profiles were fitted with a series of Gaussian peaks on a polynomial background (Peak Fit, SPSS, Chicago, IL). The RLC content of each sample was normalized by the total essential light chain content.

RESULTS

Exchange of fluorescent myosin regulatory light chains into muscle fibers

The kinetics of myosin RLC exchange into demembranated muscle fibers in EDTA rigor solution (''exchange solution'', see Methods) at 30°C were investigated using a double-cysteine mutant of chicken gizzard RLC with cysteines 100 and 108 cross-linked by BR (Corrie et al., 1998). This labeled light chain will be referred to as 100-BR-108 RLC. In our previous work, monofunctionally labeled RLCs (e.g,. Ling et al., 1996; Sabido-David et al., 1998a,b) and bifunctionally labeled RLCs (Corrie et al., 1999), were exchanged into fibers using a 30-min incubation in exchange solution at 30°C. Here we studied shorter exchange times by incubating fibers in exchange solution containing 50 μM of 100-BR-108 RLC at 10°C, raising the temperature to 30°C for 1, 3, 10, or 30 min, then cooling to 10°C for measurements of fluorescence intensity (Fig. 2, *ON* experiments). The extent of RLC exchange at 30°C estimated from the total fluorescence intensity had a large fast component with a time constant of ~4 min (Fig. 2 *A*, *ON*). RLC exchange was not detectable at 10°C.

In a separate set of experiments, 100-BR-108 RLC was introduced by a 30-min incubation at 30°C, then fibers were bathed in relaxing solution containing whole troponin and troponin C to replace any of these proteins that were lost during RLC exchange (Ling et al., 1996). The fibers were put back into rigor solution, and fluorescence intensities were measured at 10°C after incubation for 0, 1, 3, 10, 30, or 70 min at 30°C in exchange solution containing 50 μM wild-type RLC (Fig. 2, *OFF* experiments). Again there was a fast exchange component; about half of the 100-BR-108 RLC left the fiber in 3 min. However, the remaining 100-BR-108 RLC was removed from the fiber much more slowly. The fluorescence intensity decrease could be described by an exponential component with a time constant <2 min followed by a linear decrease of 0.25% min^{-1} (Fig. 2 *A*, *OFF*).

The polarization of the fluorescence after each period of RLC exchange was used to characterize the orientation of the 100-BR-108 RLC. Fibers were illuminated with light polarized either parallel or perpendicular to the fiber axis, and the intensities of fluorescence components polarized parallel and perpendicular to the fiber axis were measured for emission components propagating both in-line and at 90° to the excitation light (Hopkins et al., 1998; Dale et al., 1999; Corrie et al., 1999). Three independent order parameters related to the orientation of the BR dipole with respect to the

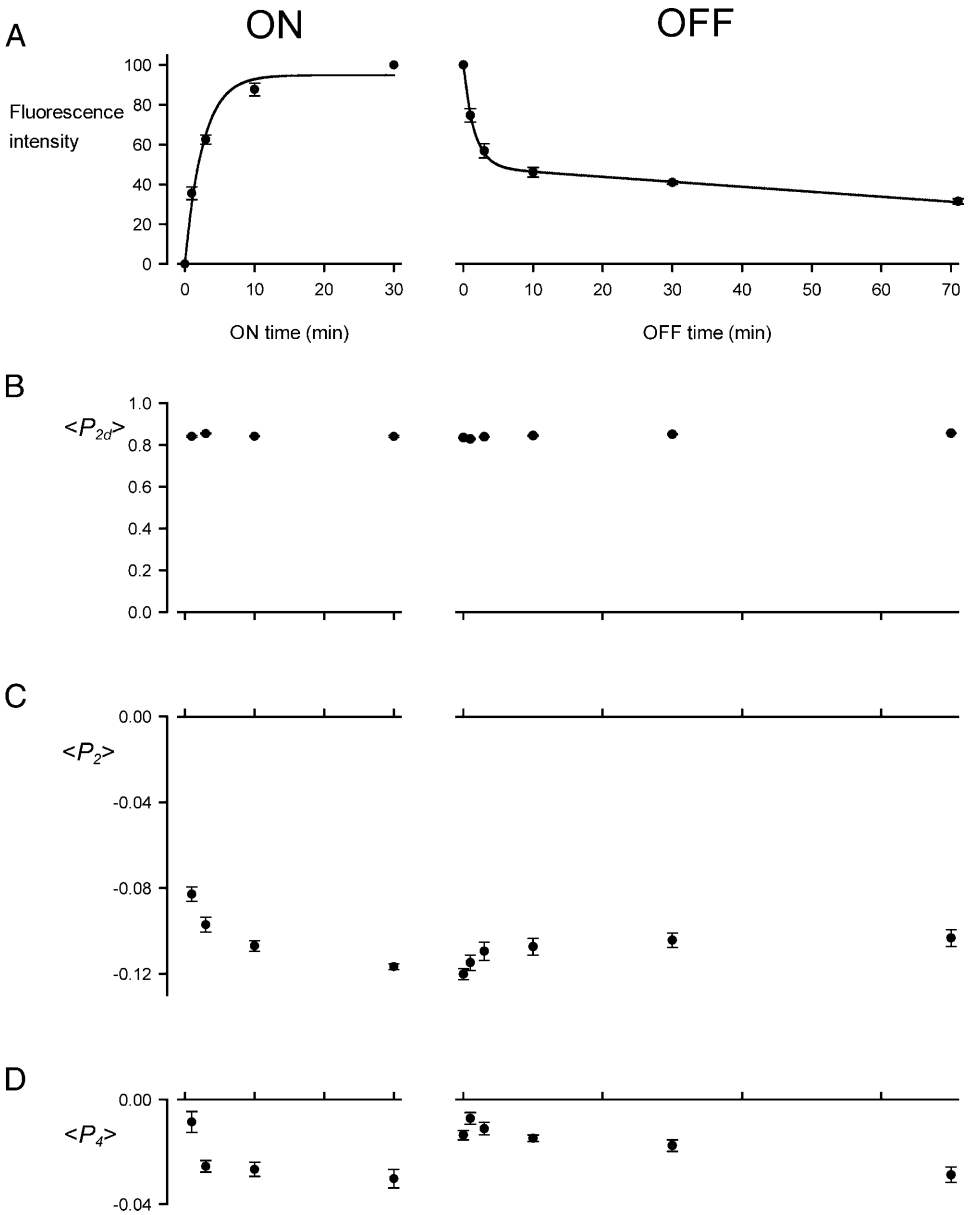

FIGURE 2 Kinetics of RLC exchange in single muscle fibers. (*A*) Total fluorescence intensity from 100-BR-108 in the fiber, normalized by the value after a 30-min exchange. (*B–D*) Order parameters $\langle P_{2d}\rangle$, $\langle P_2\rangle$, and $\langle P_4\rangle$, respectively. All measurements were made in exchange solution at 10°C. The time axis shows the duration of exchange at 30°C in the presence of 100-BR-108 RLC (*ON* experiment) or unlabeled wild-type RLC (*OFF* experiment). Mean ± SE for five fibers (*ON*) or six fibers (*OFF*); the lines in *A* are an exponential fit (*ON*) and exponential plus linear component (*OFF*).

fiber axis can be determined from these data. $\langle P_{2d}\rangle$ is the second-rank order parameter that describes the amplitude of rapid (subnanosecond) wobble of the BR dipole with respect to the protein backbone (Dale et al., 1999). $\langle P_2\rangle$ and $\langle P_4\rangle$ are the second- and fourth-rank order parameters that describe the average orientation distribution with respect to the fiber axis of the center axis of the wobble cone of the BR dipole. $\langle P_2\rangle$ depends monotonically on the average angle (θ) between the BR dipole and the fiber axis; if all the dipoles are parallel to the fiber axis ($\theta = 0°$), $\langle P_2\rangle = 1$; if they are all perpendicular to the fiber axis ($\theta = 90°$), $\langle P_2\rangle = -0.5$. Thus a decrease in $\langle P_2\rangle$ indicates that the dipoles became more perpendicular to the fiber axis. $\langle P_4\rangle$ has a more complicated dependence on θ, when $\theta = 0°$, $\langle P_4\rangle = 1$; when $\theta = 50°$, $\langle P_4\rangle = -0.43$; and when $\theta = 90°$ $\langle P_4\rangle = 0.375$. In general, disorder of the dipole orientations reduces the absolute values of $\langle P_2\rangle$ and $\langle P_4\rangle$, and an isotropic distribution of dipoles has $\langle P_2\rangle = \langle P_4\rangle = 0$.

After a 30-min exchange of 100-BR-108 RLC into the fibers, $\langle P_{2d}\rangle$ in exchange solution at 10°C was 0.841 ± 0.005 (mean ± SE, five fibers; Fig. 2 *B*), $\langle P_2\rangle$ was –0.117 ± 0.001 (Fig. 2 *C*), and $\langle P_4\rangle$ was –0.030 ± 0.003 (Fig. 2 *D*). These values are similar to those measured previously for this BR-RLC in rigor conditions, 0.877 ± 0.010, −0.117 ± 0.005, and −0.046 ± 0.011 respectively (Corrie et al., 1999). A value of $\langle P_{2d}\rangle$ close to unity indicates that the subnanosecond motion of the BR dipole has a small amplitude; if the motion is modeled as uniform wobble in a cone, $\langle P_{2d}\rangle = 0.841$

corresponds to a cone of semiangle 27°. $\langle P_{2d} \rangle$ was effectively independent of the degree of RLC exchange (Fig. 2 *B*).

The values of $\langle P_2 \rangle$ and $\langle P_4 \rangle$ after a 30-min exchange of 100-BR-108 RLC indicate a slight perpendicular orientation preference of the 100-BR-108 dipole. $\langle P_2 \rangle$ decreased during the ON experiment, and increased during the OFF experiment (Fig. 2 *C*). The timing of these changes in $\langle P_2 \rangle$ appears to be correlated with the changes in total fluorescence intensity (Fig. 2 *A*). $\langle P_4 \rangle$ did not show a clear trend, and its value at the end of the 30-min ON experiment was different from that at the start of the OFF experiment. This is probably due to a difference between the batches of fibers used for the two sets of experiments.

Sarcomeric location of BR-RLC

Fibers into which BR-RLCs had been introduced by the standard 30-min, 30°C protocol were relaxed, stretched to a sarcomere length of ~4.0 μm, and fixed for examination in the confocal microscope (see Methods for details). BR fluorescence was found to colocalize with fluorescein isothiocyanate fluorescence from a myosin heavy chain antibody, showing that the BR-RLC was predominantly located in the myosin-containing A-band of the sarcomere. The distribution of BR fluorescence intensity along the sarcomere (Fig. 3) showed a region of lower intensity in the center of the A-band, corresponding to the bare zone of the myosin filaments where there are no myosin heads. There was significant BR fluorescence intensity in the I-band region of the sarcomere, and the ratio R_{IA} of the average intensity in the I-band relative to that in the A-band was 0.126 ± 0.014, 0.173 ± 0.026, 0.183 ± 0.040, and 0.172 ± 0.024 (mean ± SD, three fibers for each RLC) for 100-BR-108, 108-BR-113, 100-BR-113, and 104-BR-115 respectively. These values should be considered as upper limits for the fraction of BR-RLC located in the I-band, because of the limited spatial resolution of the microscope. Neither R_{IA} nor total fluorescence intensity was significantly different at the surface and core of the fiber, showing that BR-RLC had become equilibrated within the fiber volume during the 30-min, 30°C exchange.

Quantification of RLC exchange by SDS-PAGE

Incorporation of BR-RLC and removal of the native RLC from single muscle fibers during the standard 30-min, 30°C exchange protocol were measured by SDS-PAGE with silver staining (Fig. 4). The BR-RLCs, which are based on the chicken gizzard RLC sequence, were readily separated from the native rabbit skeletal RLC (rsRLC) on the basis of their slower migration on the gel. After RLC exchange (lane *B*), the rsRLC band was clearly less intense than in the control fiber (lane *A*). Troponin components, in particular troponin C (lane *C*), were also lost in the RLC exchange protocol, and a new band corresponding to BR-RLC (lane *D*) appeared. The amount of BR-RLC incorporated was 0.69 ± 0.05 (mean ± SE, $n = 15$) of the total content of essential light chains (ELC1 and ELC2), which are not extracted by the RLC exchange protocol. Thus 69% of myosin heads contained a BR-RLC, and this percentage was not significantly different for 100-BR-108, 100-BR-113, 108-BR-113, and 104-BR-115 RLCs. The fraction of rsRLC extracted was 0.61 ± 0.06, consistent with stoichiometric exchange of 60–70% of BR-RLC for native RLC.

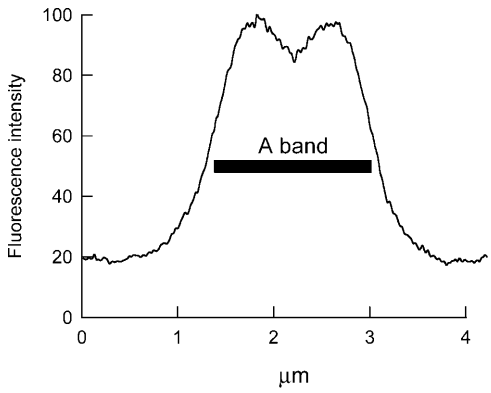

FIGURE 3 Distribution of BR fluorescence intensity along a sarcomere. Data were calculated from a single confocal image of a fiber into which 100-BR-113 RLC had been exchanged for 30 min at 30°C, averaged from four contiguous sarcomeres. Sarcomere length 4.2 μm. The bar denotes the 1.6 μm region corresponding to the A-band.

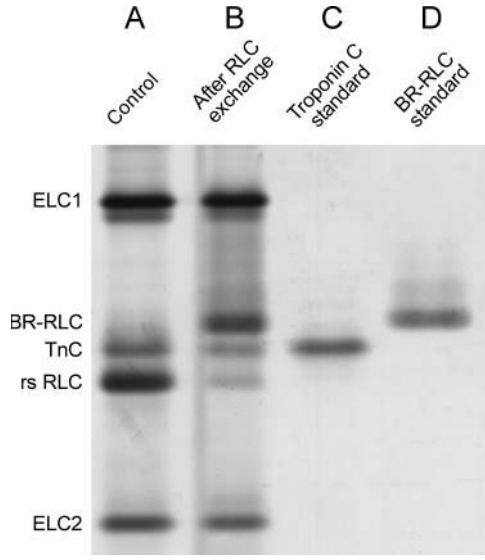

FIGURE 4 Silver stained SDS-PAGE showing effects of RLC exchange in a single fiber from rabbit psoas muscle. (*A*) Control. (*B*) After exchange of 100-BR-113 RLC for 30 min at 30°C. (*C*) Troponin C standard. (*D*) 100-BR-113 RLC standard. Lanes *A* and *B* are from two adjacent segments of the same muscle fiber.

Effect of RLC exchange on active isometric force

Replacement of 60–70% of the native RLC by BR-RLC had little effect on active isometric force. After the standard 30-min, 30°C exchange protocol, including replacement of troponin and troponin C, active isometric force was 93 ± 4% (mean ± SD, $n = 9$), 88 ± 4% ($n = 4$), 91 ± 5% ($n = 6$), and 84 ± 9% ($n = 8$) of that before exchange, for 100-BR-108, 108-BR-113, 100-BR-113, and 104-BR-115, respectively. The average isometric force at 10°C after RLC exchange was 98 ± 9 kN m^{-2}. Reduction of isometric force by ~10% seems to be a nonspecific effect of the RLC exchange protocol, and a similar reduction was reported previously for exchange of both chicken gizzard and rabbit skeletal RLCs labeled with monofunctional rhodamines (Ling et al., 1996).

Orientation of BR-RLC dipoles in relaxed muscle fibers

The order parameters $\langle P_{2d} \rangle$, $\langle P_2 \rangle$, and $\langle P_4 \rangle$ were measured after exchange of 100-BR-108, 100-BR-113, 104-BR-115, or 108-BR-113 RLC into fibers using the standard 30-min, 30°C protocol (Fig. 5). The order parameter describing local probe motion on the subnanosecond timescale, $\langle P_{2d} \rangle$, was ~0.8 for all four BR-RLCs, corresponding to wobble in a cone with semiangle ~30°, as reported previously (Corrie et al., 1999). $\langle P_{2d} \rangle$ showed no clear dependence on the temperature or ionic strength of the relaxing solution, but was slightly larger in rigor conditions, indicating a small restriction of the range of rapid probe motions compared with that observed in relaxing conditions.

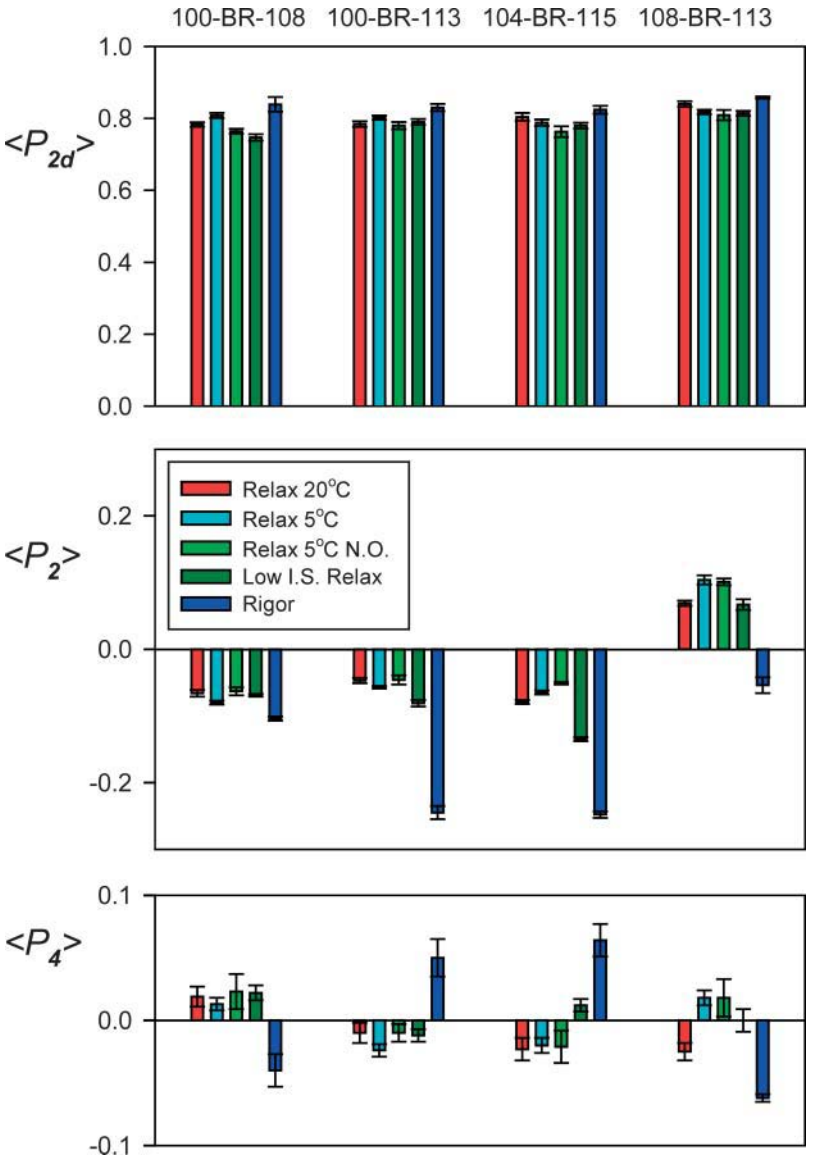

FIGURE 5 Order parameters for four BR-RLCs in relaxing and rigor conditions. Mean ± SE for $n = 4$–13 fibers. Sarcomere length 2.4 μm except for ''no overlap'' (*N.O.*) conditions, for which it was 4.0 μm. Ionic strength of relaxing solutions was 160 mM except for ''Low I.S. Relax'' conditions, for which it was 20 mM.

The order parameters $\langle P_2 \rangle$ and $\langle P_4 \rangle$, describing the static part of the orientation distribution of the BR-RLC dipoles, had a small but reproducible dependence on the temperature and ionic strength of the relaxing solution, and on the sarcomere length (Fig. 5). Larger changes were observed when fibers were put into rigor (Fig. 5, *dark blue*).

Effect of temperature

Increasing the temperature of the relaxing solution from 5°C (Fig. 5, *cyan*) to 20°C (*red*) increased $\langle P_2 \rangle$ for 100-BR-108 and 100-BR-113, and decreased $\langle P_2 \rangle$ for 104-BR-115 and 108-BR-113, suggesting that the orientation of the RLC changes so as to make the 100-BR-108 and 100-BR-113 dipoles more parallel to the fiber axis and the 104-BR-115 and 108-BR-113 dipoles more perpendicular to it. The largest change was observed for 108-BR-113, and $\langle P_4 \rangle$ for this BR-RLC also changed sign when the temperature was increased. Similar effects of temperature were observed after fibers had been stretched to sarcomere length 4.0 μm to eliminate overlap between actin- and myosin-containing filaments. For example, when temperature was increased from 10°C to 20°C in a separate set of experiments, $\langle P_2 \rangle$ for 108-BR-113 decreased by 0.023 $\pm$ 0.004 (mean $\pm$ SE, five fibers) at sarcomere length 2.4 μm and by 0.022 $\pm$ 0.005 at sarcomere length 4.0 μm. Thus the effects of temperature on RLC orientation in relaxing conditions are independent of the proximity of actin filaments, as shown previously for temperature-dependent changes in the arrangement of myosin heads on the surface of the myosin filaments observed by x-ray diffraction (Wray, 1987; Lowy et al., 1991; Xu et al., 1999).

Effect of sarcomere length

Stretching relaxed fibers from a sarcomere length of 2.4 μm, where the overlap between actin filaments and the region of the myosin filaments containing myosin heads is complete (Fig. 5, *cyan*), to sarcomere length 4.0 μm, where the overlap is almost abolished (Fig. 5, *light green*), produced a very small decrease in the absolute value of $\langle P_2 \rangle$ for each BR-RLC at 5°C, with no significant change in $\langle P_4 \rangle$. These changes suggest a slight increase in the disorder of RLC orientations when myosin heads are withdrawn from the proximity of the actin filaments, with little change in their average orientation. Similar small changes in $\langle P_2 \rangle$ were observed when fibers were stretched in relaxing solution at 20°C.

Effect of ionic strength

When the ionic strength of the relaxing solution was decreased from 160 mM (Fig. 5, *cyan*) to 20 mM (*dark green*) at sarcomere length 2.4 μm, 5°C, to promote weak binding of myosin heads to actin, $\langle P_2 \rangle$ and $\langle P_4 \rangle$ for the BR-RLC dipoles generally changed toward their respective rigor values (*dark blue*). The relative magnitudes of the changes in $\langle P_2 \rangle$ and $\langle P_4 \rangle$ associated with lowering ionic strength in relaxing solution and with the relaxed-to-rigor transition were different for the different RLCs. For example, 104-BR-115 showed a much larger ionic strength effect than 100-BR-108.

Although fiber diameter was 7.5% smaller, on average, at the lower ionic strength, the $\langle P_2 \rangle$ and $\langle P_4 \rangle$ changes were not due to compression of the filament lattice. Addition of 3% dextran T-500 (Amersham Biosciences) to the relaxing solution, which produced a similar decrease in fiber diameter, did not alter $\langle P_2 \rangle$ or $\langle P_4 \rangle$.

The effects of lowering ionic strength in relaxing solution were greatly reduced at sarcomere length 4.0 μm, where myosin heads cannot bind to actin filaments. For example, when ionic strength was lowered from 160 mM to 20 mM, $\langle P_2 \rangle$ for 104-BR-115 decreased by 0.070 $\pm$ 0.006 (mean $\pm$ SE, six fibers) at sarcomere length 2.4 μm, but increased by 0.009 $\pm$ 0.002 at sarcomere length 4.0 μm. These results show that binding to actin is required for the change in RLC orientation observed when ionic strength is lowered at the shorter sarcomere length, consistent with previous results with monofunctional RLC probes (Sabido-David et al., 1998a).

RLC orientation distributions

The major advantage of two-site attachment of orientation probes is that their dipole orientations in the protein coordinate frame are known. Thus the $\langle P_2 \rangle$ and $\langle P_4 \rangle$ values from a set of such BR-RLC dipoles can be used to determine the absolute orientation of the RLC with respect to the filament axis (Corrie et al., 1999). Here we define the RLC orientation in terms of the tilt angle β between the filament axis and the ''lever axis'', joining Cys^{707} and Lys^{843} of the myosin heavy chain (Fig. 1), and a twist angle γ that specifies rotation of the RLC around the lever axis. γ is zero when the short ''hook'' helix at the C-terminus of the myosin heavy chain in the head region is in the same plane as the filament and lever axes, with its C-terminus (Lys^{843}) pointing toward the M-line of the half-sarcomere. These definitions are the same as those used by Hopkins et al. (2002), and differ slightly from those of Corrie et al. (1999) in the definition of the lever axis. Details of the angle definitions are given in Methods.

The measured $\langle P_2 \rangle$ and $\langle P_4 \rangle$ values from the four BR-RLCs give information about the distribution of RLC orientations (β and γ) in each set of experimental conditions. If every RLC in the fiber had the same (β,γ) orientation, this could be calculated from the measured $\langle P_2 \rangle$ and $\langle P_4 \rangle$ values. In practice, there is a distribution of RLC orientations that is not uniquely determined by $\langle P_2 \rangle$ and $\langle P_4 \rangle$. In some circumstances it is useful to fit the observed $\langle P_2 \rangle$ and $\langle P_4 \rangle$ values to model orientation distributions, for example

a single Gaussian distribution or the sum of two Gaussian distributions corresponding to functionally distinct populations of myosin heads (Corrie et al., 1999; Hopkins et al., 2002). Here we used an alternative model-independent approach that requires no a priori information about the orientation distribution: maximum entropy analysis (Levine and Tribus, 1979; van der Heide et al., 2000; Hopkins et al., 2002).

The maximum entropy distribution $f_{ME}(\beta,\gamma)$ is the smoothest orientation distribution, i.e., the distribution with the greatest informational entropy, that is consistent with a given set of order parameters. $f_{ME}(\beta,\gamma)$ is an exact but not unique representation of the limited information contained in $\langle P_2\rangle$ and $\langle P_4\rangle$, and can be regarded as a low-resolution version of the real orientation distribution. The maximum entropy distributions $f_{ME}(\beta,\gamma)$ calculated from the order parameters in Fig. 5 are shown as contour plots in Fig. 6. In all conditions studied, there was a maximum value of f_{ME} close to the center of the map, i.e., near $\beta = 90°$, $\gamma = 0°$. Each map has a second maximum related to the first by the symmetry transformation ($180° - \beta$; $180° + \gamma$); this can be considered as the other end of a dipole or, equivalently, the other half of each sarcomere in the muscle fiber. The results will be described in terms of the peak near $\beta = 90°$, $\gamma = 0°$. Each f_{ME} map shows six equally spaced contour levels, scaled to the respective maximum value (the central dot).

In relaxing solution at 20°C (Fig. 6 *A*), the peak of the maximum entropy distribution of RLC orientations was at $\beta = 110°$, $\gamma = 20°$. This orientation of the RLC is depicted graphically in Fig. 1. About 40% of the density of the maximum entropy distribution in Fig. 6 *A* is within the region $80° < \beta < 140°$; $-20° < \gamma < 60°$ and its symmetry-related equivalent. An asymmetric tail of density extends from the central peak toward lower values of β and γ. At 5°C (Fig. 6 *B*), the central peak was at $\beta = 100°$, $\gamma = 0°$ and the distribution was more symmetrical. Similar effects of temperature on the shape and position of the central peak were observed in a separate set of experiments in which the temperature of relaxed fibers was increased from 10°C to 20°C at sarcomere length 4.0 μm; in those experiments the maximum of f_{ME} was at $\beta = 105°$, $\gamma = 10°$ at 10°C, and $\beta = 110°$, $\gamma = 20°$ at 20°C.

The orientation of the RLC region of the myosin heads in normal ionic strength relaxing conditions did not show a clear dependence on overlap between actin and myosin filaments. At 5°C the central peak of the f_{ME} distribution was at $\beta = 100°$, $\gamma = 0°$ both at sarcomere length 2.4 μm (Fig. 6 *B*) and at 4.0 μm (Fig. 6 *C*). Similar results were obtained in another set of experiments when sarcomere length was varied at 20°C. Thus RLC orientation in normal ionic strength relaxing conditions is not affected by the proximity of actin filaments.

In contrast, lowering the ionic strength of the relaxing solution from 160 to 20 mM at 5°C did change the f_{ME} distribution (Fig. 6 *D*). The central peak of the f_{ME} map shifted from $\beta = 100°$, $\gamma = 0°$ at 160 mM ionic strength, 5°C (Fig. 6 *C*) to $\beta = 100°$, $\gamma = 20°$ at the lower ionic strength (Fig. 6 *D*). A similar increase in γ was seen in the rigor f_{ME} distribution (Fig. 6 *E*). However, the latter has more closely

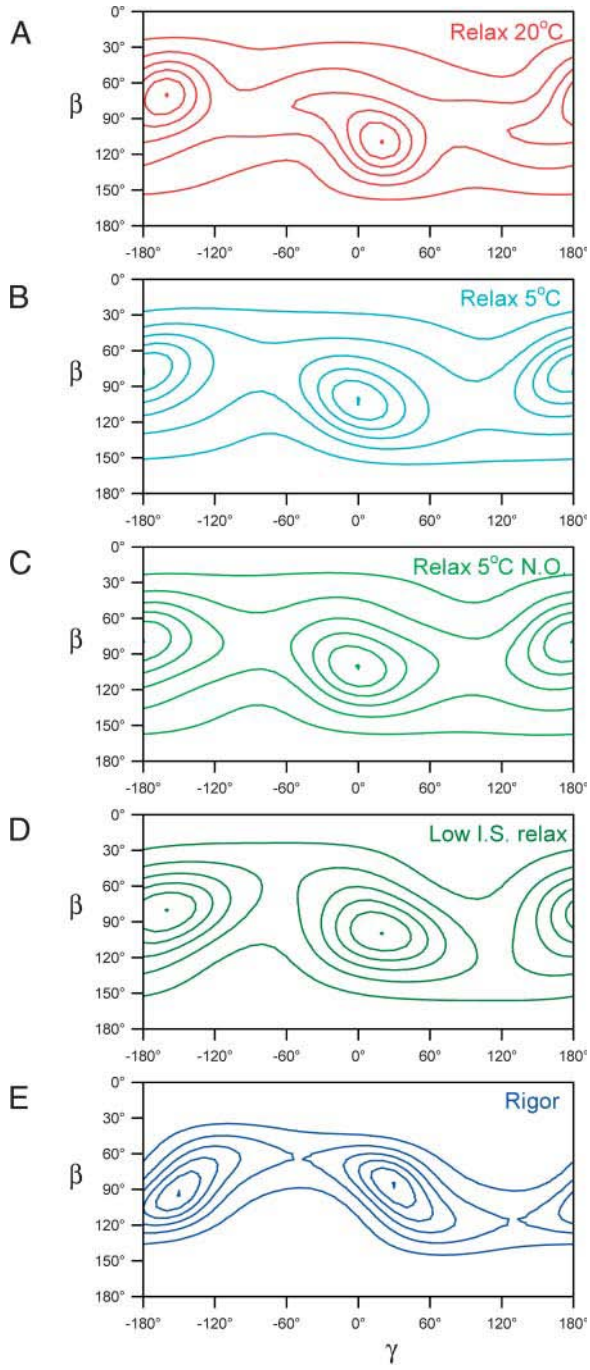

FIGURE 6 Maximum entropy orientation distributions for the RLC region in relaxing and rigor conditions. Panels *A–E* show the same five conditions as in Fig. 5. β and γ are the tilt and twist angles of the RLC region of the myosin head defined in the text. The contour lines show six equally spaced density levels, scaled to the peak of the distribution (shown as a *dot*), which had relative values 0.18, 0.17, 0.16, 0.18, and 0.27 in panels *A–E*, respectively.

spaced contours and a diagonal shape that indicates a positive correlation between β and γ (Hopkins et al., 2002). The maximum of the rigor f_{ME} distribution was at $\beta = 85°$, $\gamma = 25°$, close to the values $\beta = 80°$, $\gamma = 22°$ calculated previously from the $\langle P_2 \rangle$ and $\langle P_4 \rangle$ values for 100-BR-108, 104-BR-115, and 108-BR-113 in rigor fibers (Hopkins et al., 2002).

DISCUSSION

Exchange of BR-RLC for native RLC in single muscle fibers

The BR approach for measuring the orientation of protein domains in their native environment was introduced by Corrie et al. (1999), who also applied it to the myosin RLC in skeletal muscle fibers. Those authors described the preparation of pure 1:1 conjugates of expressed double-cysteine mutants of the RLC with BR, and showed that BR-RLCs bind normally to the myosin heavy chain and restore Ca^{2+}-regulation of the Mg^{2+}-ATPase activity of scallop myofibrils. In this work we investigated the exchange of these BR-RLCs for the native RLCs in single demembranated fibers from skeletal muscle.

The standard method of introducing exogenous RLCs into demembranated muscle fibers, used in previous studies with RLC probes (Irving et al., 1995; Ling et al., 1996; Sabido-David et al., 1998a,b; Hopkins et al., 1998, 2002; Corrie et al., 1999) employs a 30-min, 30°C incubation in an EDTA rigor solution containing the exogenous RLC. In these conditions, the binding of the RLC to the myosin heavy chain is considerably weakened, presumably as a result of removal of the Mg^{2+} ion that is normally bound to the N-terminal lobe of the RLC (Rayment et al., 1993b; Xie et al., 1994), leading to replacement of the native by the exogenous RLC.

When this method was used with 50 μM BR-RLC, ~60% of the native RLC was removed, and replaced by a roughly equal amount of BR-RLC (Fig. 4). This stoichiometry suggests that the BR-RLC binds specifically to myosin heavy chain sites from which the native RLC has been removed. This interpretation was supported by confocal microscopy of muscle fibers into which BR-RLC had been exchanged by the standard protocol, then stretched in relaxing solution to long sarcomere length. The BR-RLC fluorescence intensity from the I-bands of these stretched sarcomeres, which should not contain myosin, was only 12–18% of that from of the myosin-containing A-bands (Fig. 3). The true fraction of the BR-RLC in the I-bands is likely to be lower than this estimate because of the limited spatial resolution of the microscope.

Kinetic analysis of the exchange of 100-BR-108 RLC under these conditions (Fig. 2) revealed fast and slow components of RLC exchange. In the OFF experiment, BR-RLC bound in the fiber was replaced by unlabeled RLC, and the fast component accounted for about half the total RLC exchange. Since the fast component is effectively complete in the standard 30-min exchange period, and the slow component has progressed to only a small extent in the same period, these results suggest that about half of the native RLC is replaced by BR-RLC in the 30-min exchange, in agreement with the SDS-PAGE results (Fig. 4). The slow component of RLC exchange is unlikely to be due to slow RLC diffusion into and out of the core of the fiber, because confocal microscopy showed that there was no variation of BR-RLC fluorescence intensity through the depth of the fiber. One possible explanation for these results would be that one of the two heads of each myosin can exchange its RLC more easily than the other in EDTA rigor conditions (Simmons and Szent-Györgyi, 1980).

Whatever the origin of the fast and slow components of BR-RLC exchange, the BR dipoles of the two components have a similar orientation and mobility in the fiber, at least for the 100-BR-108 RLC studied in Fig. 2. $\langle P_{2d} \rangle$, the order parameter that describes the amplitude of subnanosecond probe wobble, was the same in the fast and slow phases (Fig. 2 *B*). The changes in $\langle P_2 \rangle$ (Fig. 2 *C*) and $\langle P_4 \rangle$ (Fig. 2 *D*) in the fast phase were small, particularly when BR-RLC was removed from the fiber in the OFF experiment. Larger changes in $\langle P_2 \rangle$ and $\langle P_4 \rangle$ were observed in the fast phase of the ON experiment, but these short ON exchange periods may result in more nonspecific BR-RLC binding than in the normal 30-min protocol if there is insufficient time for BR-RLC to diffuse to and occupy binding sites vacated by native RLC.

Taken together, the fluorescence time courses (Fig. 2), confocal microscopy (Fig. 3) and SDS-PAGE results (Fig. 4) show that the standard RLC exchange protocol (30 min at 30°C in EDTA rigor solution) specifically replaces about half of the native RLC by BR-RLC. About 10% of the BR-RLC could be bound nonspecifically in the fiber. If this component were oriented isotropically, it would reduce the measured values of $\langle P_2 \rangle$ and $\langle P_4 \rangle$ by 10% (since an isotropic distribution has $\langle P_2 \rangle = \langle P_4 \rangle = 0$). The effect of this on the calculated RLC orientation distributions was assessed by repeating the maximum entropy analysis after the measured $\langle P_2 \rangle$ and $\langle P_4 \rangle$ (Fig. 5) values had been increased by 10%. The effect on the orientation distributions was negligible, and the peak orientations changed by $<5°$.

Replacement of about half of the native RLC by BR-RLC reduced the maximum isometric force produced by the fibers by ~10%. Similar reductions have been reported previously for other exogenous RLCs introduced using the same protocol (Ling et al., 1996), and this small reduction in isometric force appears to be a general effect of the 30-min incubation at 30°C in EDTA rigor solution rather than a specific effect of the presence of the exogenous RLC. We conclude that myosin heads incorporating the BR-RLCs have the same force-producing capability as native myosin heads.

Orientation of the RLC region of myosin heads in relaxed muscle

Maximum entropy orientation distributions

Several previous studies have used fluorescence polarization to investigate the orientation of the RLC region of the myosin heads in relaxed skeletal muscle (Ling et al., 1996; Sabido-David et al., 1998a,b; Hopkins et al., 1998; Corrie et al., 1999). Corrie et al. (1999) used the same RLC exchange protocols and BR-RLCs as in this work to measure changes in orientation of the RLC region of the myosin heads during active force generation. They also reported polarized fluorescence data for relaxing solution at 10°C, 160 mM ionic strength, and fitted them with Gaussian orientation distributions. However the reduced χ^2 (with 4 degrees of freedom) for their best Gaussian fit was 7.69, suggesting that the orientation distribution of the RLC distribution in relaxed muscle does not have a Gaussian shape.

We therefore analyzed the polarized fluorescence data from the BR-RLC probes in the present experiments in terms of maximum entropy (ME) orientation distributions (van der Heide et al., 2000; Hopkins et al., 2002). Maximum entropy analysis avoids assumptions about the shape of the orientation distribution, and fits the observed order parameters exactly. The ME distributions presented above were calculated from the first two order parameters, $\langle P_2 \rangle$ and $\langle P_4 \rangle$, in an infinite series that would completely describe the real orientation distribution. If the real distribution had multiple closely spaced peaks, these would not be resolved in the ME distributions. On the other hand, simple model orientation distributions are reliably recovered by the ME analysis method used here (van der Heide et al., 2000). The resolution of ME analysis could probably be improved in future studies by using more probe attachment sites (van der Heide et al., 2000), or by measuring higher-rank order parameters ($\langle P_6 \rangle$, $\langle P_8 \rangle$, etc.) by pulsed fluorescence excitation techniques (Bell et al., 2002).

Orientation of the RLC region in relaxing solution at 20°C

The ME orientation distribution of the RLC region in relaxed muscle at 20°C has a prominent and well-defined peak centered on $\beta = 110°$, $\gamma = 20°$, with a symmetry-related equivalent at $\beta = 70°$, $\gamma = -160°$ (Fig. 6 *A*). The tail at the lower β- and γ-side of the central peak might be due to a second population of myosin heads with an RLC orientation around $\beta = 70°$, $\gamma = -50°$ (and $\beta = 110°$, $\gamma = 130°$).

The central peak of the ME distribution for relaxed muscle at 20°C corresponds to a myosin head orientation in which the hook helix (Pro^{830}–Lys^{843}) is almost parallel to the filament axis, with its Lys^{843} end pointing toward the M-line of the sarcomere, and the lever axis (Cys^{707}–Lys^{843}) at 110° to the filament axis, with its Lys^{843} end farther from the M-line (Fig. 1). In this conformation, the hook helix is likely to be almost parallel to the adjoining subfragment-2 region of the myosin rod.

X-ray diffraction (Wray, 1987; Lowy et al., 1991; Xu et al., 1997, 1999) and electron microscopy (Menetret et al., 1990; Sosa et al., 1994; Levine et al., 1998; Bennett et al., 2002) studies of fibers and myosin filaments isolated from rabbit psoas muscle have shown that the myosin heads have a quasihelical organization on the surface of the myosin filaments in relaxing conditions at 20°C. The resolution of those studies was not sufficient to reveal the conformation of individual myosin heads or the details of the intermolecular packing interactions that stabilize the structure. However, modeling of the x-ray diffraction pattern under the assumption of helical symmetry suggests that the two heads wrap around the filaments with their long axes at ~80° and 115° to the filament axis (Malinchik et al., 1997), similar to the peak conformations of the lever axis deduced from the BR-RLC probes (Figs. 1 and 6 *A*). The x-ray diffraction pattern from resting fish muscle has been modeled in terms of myosin head orientations without the constraint of helical symmetry (Hudson et al., 1997), and the best-fit model had six distinct head orientations with a range of axial tilts of ~70°. The average tilt angle was again almost perpendicular to the filament axis. Thus the maximum entropy distribution of the orientation of the RLC regions of the myosin heads is broadly consistent with the quasihelical order of the myosin heads in relaxed muscle deduced from x-ray diffraction studies, although detailed comparisons are not yet possible.

Effect of temperature on the orientation of the RLC region in relaxed muscle

Lowering the temperature of the relaxing solution from 20°C to 5°C produced small but reproducible changes in the order parameters from the BR-RLC probes (Fig. 5). The effect on the maximum entropy distribution of RLC orientations (Fig. 6, *A* and *B*) was correspondingly subtle. The relatively sharp distribution, peaking at $\beta = 110°$, $\gamma = 20°$, that was observed at 20°C (Fig. 6 *A*) became rather broader and more symmetric at 5°C (Fig. 6 *B*) and the peak was at $\beta = 110°$, $\gamma = 0°$. The modest effect of the temperature of the relaxing solution on the orientation of the RLC region contrasts with its marked effect on the x-ray diffraction pattern in the same temperature range (Wray, 1987; Lowy et al., 1991; Xu et al., 1997, 1999). The quasihelical order of the myosin heads on the surface of the myosin filaments is much more marked at 20°C than at 5°C. Changes in the intensities of the equatorial x-ray reflections (Peckham and Irving, 1989; Xu et al., 1997) and modeling of the myosin-based layer lines (Malinchik et al., 1997) in the same temperature range suggest that the heads also swing out from the surface of the myosin filament at the lower temperature. Thus the change in quasihelical order may have contributions from both azimuthal motions of the myosin heads around the filament axis and radial translation of the heads. Steady-state polarized fluorescence

measurements on muscle fibers are not sensitive to either azimuthal reorientation or translational motions.

Effect of ionic strength on the orientation of the RLC region in relaxed muscle

Lowering the ionic strength of the relaxing solution from 160 mM to 20 mM at 5°C gave rise to reproducible changes in the BR-RLC order parameters (Fig. 5), but had relatively little effect on the maximum entropy distribution of RLC orientations (Fig. 6, *B* and *D*). The ME distribution of lever arm orientations (β) was effectively independent of ionic strength. This observation seems inconsistent with the hypothesis that myosin heads bind to actin in a stereospecific conformation in low ionic strength relaxing conditions. Substantial disorder and mobility of this low ionic strength weak binding state have also been inferred from x-ray (Xu et al., 1997) and electron paramagnetic resonance (Fajer et al., 1991) fiber studies, and from electron microscopy of isolated myosin head fragments weakly bound to actin filaments (Craig et al., 1985). The increase of the twist angle γ by $\sim 20^{\circ}$ when ionic strength was lowered to 20 mM in relaxing conditions (Fig. 6 *D*) may nevertheless reflect a net change in myosin head orientation required for binding to actin within the structural constraints of the filament lattice, since a similar increase is observed in the transition from relaxation to rigor (Fig. 6 *E*).

Limitations of the bifunctional rhodamine-polarized fluorescence technique

Polarized fluorescence from bifunctional probes provides information about the local orientation distributions of the whole population of labeled molecules, including any disordered components. In common with other extrinsic probe techniques, the method is potentially vulnerable to modification of the structure or function of the target molecule by the probe. We have shown that the BR-RLCs can replace about half of the native RLCs in a skeletal muscle fiber with no significant effect on contractile function. The ability of the BR-RLCs to restore Ca^{2+} regulation of the ATPase of scallop myofibrils from which the native RLC had been extracted (Corrie et al., 1999) argues that the BR-RLCs do not affect the native structure of the RLC region. However, it remains possible that the BR-RLCs alter the structure or function of the myosin filaments in ways that would not have been detected by the above assays.

The orientation information obtained by the bifunctional rhodamine-polarized fluorescence technique is incomplete in three respects. First, there is an up-down ambiguity with respect to the symmetry axis (the actin filament axis in muscle) that results in two equivalent peaks in each maximum entropy distribution (Fig. 6). For the RLC region, this ambiguity can be resolved in experiments in which filament sliding is imposed (Corrie et al., 1999; Hopkins et al., 2002). Second, the orientational resolution is limited to the information contained in the first two order parameters, as discussed above in relation to maximum entropy analysis. Third, changes in the azimuthal orientation distribution of the probes around the symmetry axis cannot usually be deduced from steady-state polarized fluorescence measurements. Some of these limitations may be removed by further developments of the technique (van der Heide et al., 2000; Bell et al., 2002).

In many respects the information about myosin head conformations that can be gleaned from polarized fluorescence studies is complementary to that obtained by x-ray diffraction and electron microscopy. The latter techniques emphasize the ordered components of the structure, and yield a relatively low resolution view of the three-dimensional mass distribution of these ordered components, which could provide the azimuthal information that cannot be obtained by steady-state fluorescence polarization studies. Electron microscopy should be able to resolve the up-down ambiguity in the interpretation of data from x-ray and dipole probe techniques. X-ray diffraction and electron microscopy could also be used to assess possible structural modifications induced by BR-RLC exchange.

We are grateful to J. E. T. Corrie, D. R. Trentham, and J. Kendrick-Jones for help and advice throughout the course of the work, to them and to Y. E. Goldman for helpful comments on the manuscript, and to Y.-B. Sun for help with Fig.1.

Bifunctional rhodamine was a generous gift of J. E. T. Corrie and V. R. N. Munasinghe. This work was supported by the Medical Research Council, Biotechnology and Biology Research Council, and the Wellcome Trust, UK.

REFERENCES

Bell, M. G., R. E. Dale, U. A. van der Heide, and Y. E. Goldman. 2002. Polarized fluorescence depletion reports orientation distribution and rotational dynamics of muscle cross-bridges. *Biophys. J.* 83:1050–1073.

Bennett, P. M., A. Tsaturyan, and S. Bershitsky. 2002. Rapid cryofixation of rabbit muscle fibres after a temperature jump. *J. Microsc.* 206: 152–160.

Corrie, J. E. T., J. S. Craik, and V. R. N. Munasinghe. 1998. A homobifunctional rhodamine for labeling proteins with defined orientations of a fluorophore. *Bioconjug. Chem.* 9:160–167.

Corrie, J. E. T., B. D. Brandmeier, R. E. Ferguson, D. R. Trentham, J. Kendrick-Jones, S. C. Hopkins, U. A. van der Heide, Y. E. Goldman, C. Sabido-David, R. E. Dale, S. Criddle, and M. Irving. 1999. Dynamic measurement of myosin light-chain-domain tilt and twist in muscle contraction. *Nature.* 400:425–430.

Craig, R., L. E. Greene, and E. Eisenberg. 1985. Structure of the actin-myosin complex in the presence of ATP. *Proc. Natl. Acad. Sci. USA.* 82:3247–3251.

Dale, R. E., S. C. Hopkins, U. A. van der Heide, T. Marszalek, M. Irving, and Y. E. Goldman. 1999. Model-independent analysis of the orientation of fluorescent probes with restricted mobility in muscle fibers. *Biophys. J.* 76:1606–1618.

Dominguez, R., Y. Freyzon, K. M. Trybus, and C. Cohen. 1998. Crystal structure of a vertebrate smooth muscle myosin motor domain and its complex with the essential light chain: visualization of the pre-power stroke state. *Cell.* 94:559–571.

Eisenberg, E., and T. L. Hill. 1985. Muscle contraction and free energy transduction in biological systems. *Science*. 227:999–1006.

Fajer, P., E. A. Fajer, M. Schoenberg, and D. D. Thomas. 1991. Orientational disorder and motion of weakly attached cross-bridges. *Biophys. J*. 60:624–649.

Geeves, M. A., and K. C. Holmes. 1999. Structural mechanism of muscle contraction. *Annu. Rev. Biochem*. 68:687–728.

Gill, S. C., and P. von Hippel. 1989. Calculation of protein extinction coefficients from amino acid sequence data. *Anal. Biochem*. 182: 319–326.

Giulian, G. G., R. L. Moss, and M. L. Greaser. 1983. Improved methodology for analysis and quantitation of proteins on one-dimensional silver stained slab gels. *Anal. Biochem*. 129:277–287.

Griffin, B. A., S. R. Adams, and R. Y. Tsien. 1998. Specific covalent labeling of recombinant protein molecules inside live cells. *Science*. 281:269–272.

Hopkins, S. C., C. Sabido-David, J. E. T. Corrie, M. Irving, and Y. E. Goldman. 1998. Fluorescence polarization transients from rhodamine isomers on the myosin regulatory light chain in skeletal muscle fibers. *Biophys. J*. 74:3093–3110.

Hopkins, S. C., C. Sabido-David, U. A. van der Heide, R. E. Ferguson, B. D. Brandmeier, R. E. Dale, J. Kendrick-Jones, J. E. T. Corrie, D. R. Trentham, M. Irving, and Y. E. Goldman. 2002. Orientation changes of the myosin light chain domain during filament sliding in active and rigor muscle. *J. Mol. Biol*. 318:1275–1291.

Hudson, L., J. J. Harford, R. C. Denny, and J. M. Squire. 1997. Myosin head configuration in relaxed fish muscle: resting state myosin heads must swing axially by up to 150Å or turn upside down to reach rigor. *J. Mol. Biol*. 273:440–455.

Irving, M., T. St. Claire Allen, C. Sabido-David, J. S. Craik, B. Brandmeier, J. Kendrick-Jones, J. E. T. Corrie, D. R. Trentham, and Y. E. Goldman. 1995. Tilting of the light chain region of myosin during step length changes and active force generation in skeletal muscle. *Nature*. 375:688–691.

Kraft, T., J. M. Chalovich, L. C. Yu, and B. Brenner. 1995. Parallel inhibition of active force and relaxed fiber stiffness by caldesmon fragments at physiological ionic strength and temperature conditions: additional evidence that weak cross-bridge binding to actin is an essential intermediate for force generation. *Biophys. J*. 68:2404–2418.

Levine, R. J. C., Z. Yang, N. D. Epstein, L. Fananapazir, J. T. Stull, and H. L. Sweeney. 1998. Structural and functional responses of mammalian thick filaments to alterations in myosin regulatory light chains. *J. Struct. Biol*. 122:149–161.

Levine, R. D., and M. Tribus. 1979. The maximum entropy formalism. MIT Press, Cambridge, MA. 1–14.

Ling, N., C. Shrimpton, J. Sleep, J. Kendrick-Jones, and M. Irving. 1996. Fluorescent probes of the orientation of myosin regulatory light chains in relaxed, rigor, and contracting muscle. *Biophys. J*. 70:1836–1846.

Lowy, J., D. Popp, and A. A. Stewart. 1991. X-ray studies of order-disorder transitions in the myosin heads of skinned rabbit psoas muscles. *Biophys. J*. 60:812–824.

Malinchik, S., S. Xu, and L. C. Yu. 1997. Temperature-induced structural changes in the myosin thick filament of skinned rabbit psoas muscle. *Biophys. J*. 73:2304–2312.

Mercier, P., R. E. Ferguson, M. Irving, J. E. T. Corrie, D. R. Trentham, and B. D. Sykes. 2003. The NMR structure of a bifunctional rhodamine labeled troponin C in complex with the regulatory ''switch'' peptide from troponin I; implications for *in situ* fluorescence studies in muscle fibers. *Biochemistry*. 15:4333–4348.

Menetret, J. F., R. R. Schroeder, and W. Hofmann. 1990. Cryo-electron microscopic studies of relaxed striated muscle thick filaments. *J. Muscle Res. Cell Motil*. 11:1–11.

Moss, R. L., G. G. Giulian, and M. L. Greaser. 1983. Effects of EDTA treatment upon the protein subunit composition and mechanical properties of mammalian skeletal muscle fibers. *J. Cell Biol*. 96:970–978.

Peckham, M., and M. Irving. 1989. Myosin crossbridge orientation in demembranated muscle-fibers studied by birefringence and x-ray diffraction measurements. *J. Mol. Biol*. 210:113–126.

Rayment, I., H. M. Holden, M. Whittaker, C. B. Yohn, M. Lorenz, K. C. Holmes, and R. A. Milligan. 1993a. Structure of the actin-myosin complex and its implications for muscle contraction. *Science*. 261:58–65.

Rayment, I., W. R. Rypniewski, K. Schmidt-Base, R. Smith, D. R. Tomchick, M. M. Benning, D. A. Winkelman, G. Wesenberg, and H. M. Holden. 1993b. Three dimensional structure of myosin subfragment-1: a molecular motor. *Science*. 261:50–58.

Sabido-David, C., B. D. Brandmeier, J. S. Craik, J. E. T. Corrie, D. R. Trentham, and M. Irving. 1998a. Steady-state fluorescence polarization studies of the orientation of myosin regulatory light chains in single skeletal muscle fibers using pure isomers of iodoacetamidotetramethylrhodamine. *Biophys. J*. 74:3083–3092.

Sabido-David, C., S. C. Hopkins, L. D. Saraswat, S. Lowey, Y. E. Goldman, and M. Irving. 1998b. Orientation changes of fluorescent probes at five sites on the myosin regulatory light chain during contraction of single skeletal muscle fibers. *J. Mol. Biol*. 279:387–402.

Simmons, R. M., and A. G. Szent-Györgyi. 1980. Control of tension development in scallop muscle fibres with foreign regulatory light chains. *Nature*. 286:626–628.

Sosa, H., D. Popp, G. Ouyang, and H. E. Huxley. 1994. Ultrastructure of skeletal muscle fibers studied by a plunge quick freezing method: myofilament lengths. *Biophys. J*. 67:283–292.

Taylor, J. W., J. Ott, and F. Eckstein. 1985. The rapid generation of oligonucleotide-directed mutations at high-frequency using phosphorothioate-modified DNA. *Nucleic Acids Res*. 13:8765–8785.

van der Heide, U. A., S. C. Hopkins, and Y. E. Goldman. 2000. A maximum entropy analysis of protein orientations using fluorescence polarization data from multiple probes. *Biophys. J*. 78:2138–2150.

Winder, S. J., and J. Kendrick-Jones. 1995. Protein production in three different expression vectors from a single polymerase chain-reaction product. *Anal. Biochem*. 231:271–273.

Wray, J. S. 1987. Structure of relaxed myosin filaments in relation to nucleotide state in vertebrate skeletal muscle. *J. Muscle Res. Cell Motil*. 8:62a. (Abstr.)

Xie, X., D. H. Harrison, I. Schlichting, R. M. Sweet, V. N. Kalabokis, A. G. Szent-Györgyi, and C. Cohen. 1994. Structure of the regulatory domain of scallop myosin at 2.8 Å resolution. *Nature*. 368:306–312.

Xu, S., S. Malinchik, D. Gilroy, T. Kraft, B. Brenner, and L. C. Yu. 1997. X-ray diffraction studies of cross-bridges weakly bound to actin in relaxed skinned fibers of rabbit psoas muscle. *Biophys. J*. 73:2292–2303.

Xu, S., J. Gu, T. Rhodes, B. Belknap, G. Rosenbaum, G. Offer, H. White, and L. C. Yu. 1999. The M·ADP·Pi state is required for helical order in the thick filaments of skeletal muscle. *Biophys. J*. 77:2665–2676.